

Observation of oscillatory Raman gain associated with two-photon Rabi oscillations of nanofiber-coupled atoms

Christian Liedl¹ , Sebastian Pucher¹ , Philipp Schneeweiss¹ , Leonid P Yatsenko²  and Arno Rauschenbeutel^{1,*} 

¹ Department of Physics, Humboldt-Universität zu Berlin, Unter den Linden 6, 10099 Berlin, Germany

² Institute of Physics, National Academy of Sciences of Ukraine, prospect Nauki 46, Kyiv-39 03650, Ukraine

E-mail: arno.rauschenbeutel@hu-berlin.de

Received 1 July 2022, revised 18 October 2022

Accepted for publication 20 October 2022

Published 10 November 2022



Abstract

Quantum emitters with a Λ -type level structure enable numerous protocols and applications in quantum science and technology. Understanding and controlling their dynamics is, therefore, one of the central research topics in quantum optics. Here, we drive two-photon Rabi oscillations between the two ground states of cesium atoms and observe the associated oscillatory Raman gain and absorption that stems from the atom-mediated coherent photon exchange between the two drive fields. The atoms are efficiently and homogeneously coupled with the probe field by means of a nanofiber-based optical interface. We study the dependence of the two-photon Rabi frequency on the system parameters and observe Autler–Townes splitting in the probe transmission spectrum. Beyond shedding light on the fundamental processes underlying two-photon Rabi oscillations, our method could also be used to investigate (quantum) correlations between the two drive fields as well as the dynamical establishment of electromagnetically induced transparency.

Keywords: coherent manipulation, three-level system, two-photon Rabi oscillations, Raman gain, nanophotonic interface, nanofiber

 Supplementary material for this article is available [online](#)

(Some figures may appear in colour only in the online journal)

1. Introduction

Quantum emitters with a Λ -type level structure play a central role in quantum optics. Suitably driving the two allowed optical transitions, ground-state coherences and populations can be controlled and manipulated. This enables, e.g., stimulated

Raman adiabatic passages [1, 2] and coherent population trapping [3]. Moreover, the optical response of an ensemble of Λ -type emitters can be tailored, leading to, e.g., electromagnetically-induced transparency (EIT) [4], as well as slow and stored light [5, 6]. In all these examples, the driven ensemble closely follows its steady state. The transient dynamics is nevertheless relevant, e.g., to the ultimate efficiency and fidelity of these coherent processes and protocols.

Two-photon Rabi oscillations between the two ground states of Λ -type emitters are a prime example of such transient dynamics [7]. In order to observe them, one typically exposes

* Author to whom any correspondence should be addressed.

 Original content from this work may be used under the terms of the [Creative Commons Attribution 4.0 licence](#). Any further distribution of this work must maintain attribution to the author(s) and the title of the work, journal citation and DOI.

the emitters to a two-photon Rabi pulse with varying duration, followed by a read-out of the ground-state populations [8, 9]. This method does, however, not give access to the concomitant coherent dynamics of the driving light fields. Their atom-mediated coherent photon exchange manifests as oscillatory Raman gain and absorption, where gain of one field is accompanied by absorption of the other.

In order to observe this coherent gain and absorption dynamics, one has to maximize the atom number as well as the atom–light coupling strength. Moreover, the two-photon Rabi frequency has to be well defined, meaning that each atom has to be exposed to the same light intensity. In a typical experimental situation, where an atomic ensemble couples to free-space laser beams, these requirements are challenging to meet simultaneously. To our knowledge, an oscillatory Raman gain associated with two-photon Rabi oscillations has therefore not yet been observed. In this context, coupling atoms to guided light fields in nanophotonic structures may turn out advantageous as it allows for efficient and homogeneous coupling of atomic ensembles [10].

Such a waveguide quantum electrodynamics platform can, for example, be implemented with laser-cooled atoms coupled to optical nanofibers [11–13]. In spite of the close vicinity of the nanofiber surface, ground-state decoherence times on the order of milliseconds have been experimentally demonstrated for nanofiber-coupled atoms [14]. Experiments employing a Λ -type level structure in this setting include, e.g., EIT-based light storage [15, 16], Raman cooling [17, 18], generation of single collective excitations [19], probing of the in-trap atomic motion [20], and non-reciprocal Raman amplification [21].

Here, we observe an Autler–Townes splitting in the transmission spectrum of the guided probe field, allowing us to calibrate the Rabi frequency of the coupling laser field. We then drive two-photon Rabi oscillations of a nanofiber-coupled ensemble of atoms using a nanofiber-guided probe field and a free-space coupling field. We observe an oscillatory Raman gain of the probe, which accompanies the two-photon Rabi oscillations. Finally, we experimentally confirm that the two-photon Rabi frequency scales as expected with the probe power and the two-photon detuning. This allows us to infer the atomic coupling strength to the nanofiber-guided mode.

2. Method and experimental setup

Figure 1(a) schematically shows the core elements of our experimental setup. We optically trap and interface cesium (Cs) atoms using the evanescent field of an optical nanofiber (500 nm nominal diameter) that is implemented as the waist of a tapered optical fiber. We use two nanofiber-guided trapping laser fields to form two diametral arrays of trapping sites along the nanofiber [22]. The blue-detuned running wave trapping field has a wavelength of 760 nm and a power of 20.5 mW. The red-detuned, standing wave trapping field has a wavelength of 1064 nm and a total power of 2.4 mW. Both trapping fields are far off resonance with respect to all atomic transitions. The

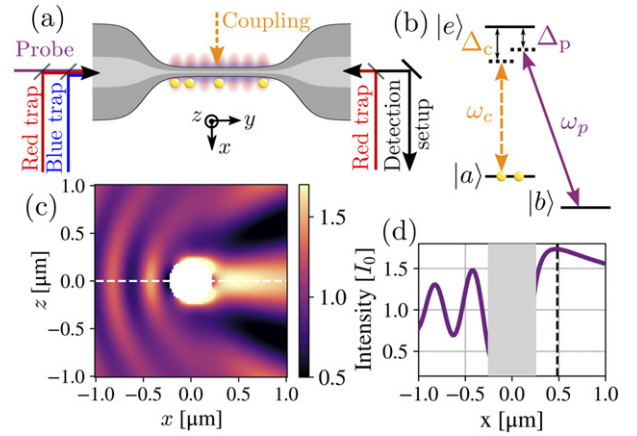


Figure 1. (a) Schematic of the experimental setup. Cs atoms (yellow spheres) are optically trapped and interfaced using the evanescent field of the nanofiber waist of a tapered optical fiber. A nanofiber-guided probe laser field and a free-space coupling laser field drive the atoms. We detect the transmitted probe power using two single-photon counting modules (not shown). A magnetic offset field is applied along the $+z$ -direction. (b) The relevant Cs energy levels form a Λ system with two ground states, $|a\rangle$ and $|b\rangle$, and an excited state $|e\rangle$. The coupling- and probe laser fields with frequencies ω_c and ω_p are detuned by Δ_c and Δ_p from the excited state, respectively. (c) Intensity distribution in the x – z plane of the coupling laser beam in the vicinity of the nanofiber. At large distances from the nanofiber, the coupling light can be approximated as a plane wave with intensity I_0 , a linear polarization along z , and a wave vector pointing into the $+x$ -direction. (d) Intensity along the white dashed line shown in panel (c). In front of the nanofiber (left half of the panel), the scattered field features a standing wave pattern due to the reflection off the nanofiber. Behind the nanofiber (right half of the panel), the light is focused, and its intensity is enhanced by a factor of about 1.7 at the position of the atoms, indicated by the black vertical line.

minima of the resulting trapping potential are located about 230 nm from the nanofiber surface.

We probabilistically load Cs atoms into the trapping potential from a magneto-optical trap using an optical molasses stage [22]. Due to the collisional blockade effect, there is at most one atom per trapping site [23]. The atoms on one side of the nanofiber are then further cooled by degenerate Raman cooling using a nanofiber-guided laser field that is near-resonant with the Cs D2 cycling transition [18]. Simultaneously, the atoms on the other side are subject to degenerate Raman heating and are thus expelled from the trap. After these steps, we switch off all cooling laser fields and are left with a one-dimensional array of a few 100 atoms in the $|a\rangle = |6S_{1/2}, F = 4, m_F = -4\rangle$ state, marking the initial setting for all experiments described below. Each sequence takes about 2 s, where most of the time is spent loading the MOT and transferring atoms to the optical dipole trap.

In each run, we determine the optical depth of the trapped ensemble by scanning the fiber-guided probe field over the D2 cycling transition and fitting the resulting transmission spectrum to a saturated Lorentzian absorption profile. We can illuminate the atoms with a free-space coupling laser field propagating in the $+x$ -direction. In order to estimate the

coupling laser intensity at the position of the atoms, we assume an incident plane wave with intensity I_0 that propagates in the $+x$ -direction and is linearly polarized along z . We analytically compute the intensity distribution of the scattered field around the nanofiber, see figure 1(c) [24, 25]. Figure 1(d) shows a cut through the intensity distribution along x for $z = 0$. The black dashed line indicates the location of the trapped atoms. Behind the fiber (right half of panel (d)), the intensity of the diffracted coupling laser beam has a maximum close to the position of the trapped atoms. Thus, the latter are exposed to an approximately constant coupling laser intensity even when considering the thermal motion of the atoms in the trap (FWHM of about 100 nm for a temperature of 30 μK). Due to the focusing effect of the nanofiber, the atoms are exposed to an intensity that is about 1.7 times larger than I_0 at the position of the trap minima, according to our calculation.

In order to stabilize the atomic population in $|a\rangle$ and suppress spin flips due to spin-motion coupling [26], we apply a magnetic offset field in the $+z$ -direction. The relevant energy levels form a Λ system, see figure 1(b). The coupling laser field drives the transition between ground state $|a\rangle$ and excited state $|e\rangle = |6P_{3/2}, F' = 4, m_{F'} = -4\rangle$, whereas the guided probe field couples the same excited state with the ground state $|b\rangle = |6S_{1/2}, F = 3, m_F = -3\rangle$. The coupling field is π -polarized, has a Rabi frequency Ω_c , and is detuned by $\Delta_c = \omega_c - \omega_{ae}$ from the $|a\rangle \rightarrow |e\rangle$ transition. Here, ω_c denotes the coupling laser frequency and ω_{ae} the transition frequency, where the latter includes all light shifts induced by the far off-resonant trapping laser fields. We note that we have attached a glossary containing the definitions and descriptions of all quantities in the supplementary material. The probe field with Rabi frequency Ω_p is phase-locked to the coupling field. It is detuned by $\Delta_p = \omega_p - \omega_{be}$ from the $|b\rangle \rightarrow |e\rangle$ transition and predominantly σ^- -polarized at the position of the atoms [25]. As for the coupling transition, ω_p and ω_{be} denote the probe laser frequency and the transition frequency, respectively. Both $|a\rangle \rightarrow |e\rangle$ and the $|b\rangle \rightarrow |e\rangle$ are transitions of the Cs D2 line at 852 nm ($\omega_{ae} \approx \omega_{be} \approx 2\pi \times 352$ THz). However, the hyperfine splitting of $\omega_{be} - \omega_{ae} \approx 2\pi \times 9.2$ GHz is much larger than the detunings Δ_p and Δ_c , as well as the natural linewidth of the transitions, such that cross-coupling can be neglected. The excited state $|e\rangle$ has a natural decay rate of $\Gamma = 2\pi \times 5.2$ MHz and decays to $|a\rangle$ and $|b\rangle$ with branching ratios of 7/15 and 5/12, respectively. With a probability of $7/60 \approx 0.1$, $|e\rangle$ decays to $|6S_{1/2}, F = 4, m_F = -3\rangle$, such that the three-level system is not closed. However, this does not substantially affect the dynamics on the short timescale we are interested in, which is why we neglect it in the following.

3. Results and discussion

3.1. Autler–Townes splitting

We now turn on the freely propagating coupling field with a Gaussian intensity profile and a peak intensity of $I_0 \approx 25$ mW cm $^{-2}$ such that almost all atoms are transferred to $|b\rangle$. After 0.1 ms, we additionally turn on a weak, fiber-guided

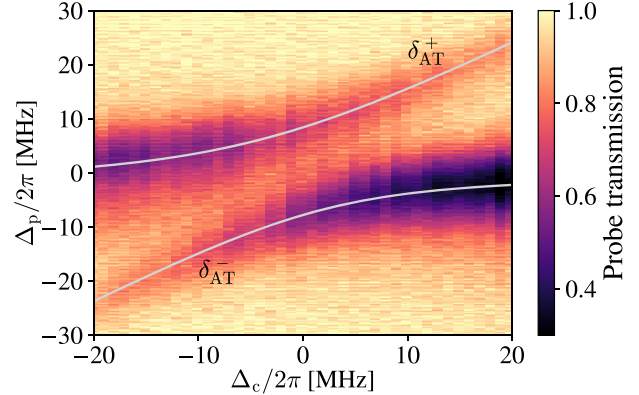


Figure 2. Probe transmission spectra for different coupling laser detunings. Two resonances are clearly visible in each spectrum, showing an avoided crossing. By fitting the frequency difference of the two resonances using the prediction based on the Autler–Townes effect (solid gray lines), we find a coupling laser Rabi frequency of $\Omega_c = 16.1(1)$ MHz. Each spectrum for a given Δ_c is averaged over 500 frequency scans of Δ_p .

probe field (saturation parameter of about 0.1) and scan its detuning Δ_p over 60 MHz in about 700 μs . This yields a transmission spectrum for a given detuning, Δ_c , of the coupling laser field. Then, we repeat the measurement for various Δ_c . The resulting transmission spectrum as a function of Δ_p and Δ_c is plotted as a colormap in figure 2.

We observe an avoided crossing of two resonances which can be explained by the Autler–Townes effect [27–29]: the strong driving of the atoms by the coupling laser field on the $|a\rangle \rightarrow |e\rangle$ transition mixes the bare states so that new eigenstates are formed. The energies of those states are split and shifted from $|e\rangle$ by [4]

$$\delta_{\text{AT}}^{\pm} = \frac{1}{2} \left(\Delta_c \pm \sqrt{\Omega_c^2 + \Delta_c^2} \right). \quad (1)$$

We fit the measured spectra to a double Lorentzian line shape and extract the splitting between the two resonance centers for each Δ_c . We then fit the splitting as a function of Δ_c using equation (1), yielding a coupling laser Rabi frequency of $\Omega_c = 2\pi \times 16.1(1)$ MHz. This is in reasonable agreement with the expected $2\pi \times 15.4$ MHz estimated from the power and diameter of the coupling laser beam used in the experiment and the calculated intensity pattern around the nanofiber. The location of the two resonances assuming the fitted Ω_c is in excellent agreement with the data and displayed as the solid gray lines in figure 2. For large Δ_c , one of the resonances converges to $\Delta_p \simeq \Delta_c$. In the following, we will denote the probe detuning from this light-shifted two-photon resonance as $\tilde{\delta} = \Delta_p - \delta_{\text{AT}}^+$.

3.2. Effective two-level system

If one chooses large detunings Δ_p and Δ_c , and two-photon detunings $\tilde{\delta} \approx 0$, such that state $|e\rangle$ is almost unpopulated, then the excited state can be adiabatically eliminated and the Λ system can effectively be described by a two-level system

[4, 30]. These effective two-level atoms can then undergo coherent two-photon Rabi oscillations between the two ground states $|a\rangle$ and $|b\rangle$, where the two-photon Rabi frequency is given by

$$\tilde{\Omega} = \frac{\Omega_p \Omega_c}{2\Delta_c}. \quad (2)$$

The incoherent one-photon scattering of the coupling field that gives rise to a residual population of the excited state and a subsequent decay can be described by introducing an effective decay rate $\tilde{\Gamma}$ for the effective two-level system from $|a\rangle$ to $|b\rangle$

$$\tilde{\Gamma} = \frac{1}{8} \frac{|\Omega_c|^2}{\Delta_c^2} \Gamma. \quad (3)$$

The one-photon scattering of the probe field would correspond to a decay from $|b\rangle$ to $|a\rangle$ in the effective two-level model. However, the one-photon scattering rate of the probe field is small compared to the one-photon scattering rate of the coupling field for our settings, $\Omega_p^2/\Omega_c^2 \approx 0.05$, which is why we only take into account the latter in our model. A more detailed description of the adiabatic elimination can be found in the supplementary material. In order to maximize the modulation of the probe transmission caused by Raman gain and absorption, the probe power, and hence, its Rabi frequency should be as small as possible. However, in the absence of technical dephasing, a necessary requirement to see oscillations is $\tilde{\Omega} > \tilde{\Gamma}$. Using equations (2) and (3), this condition translates to a requirement for the probe Rabi frequency:

$$\Omega_p > \frac{\Omega_c \Gamma}{4\Delta_c}. \quad (4)$$

The single-atom dynamics for resonant driving can be described analytically [31] using the parameters Rabi frequency $\tilde{\Omega}$, decay rate $\tilde{\Gamma}$ and decoherence rate $\gamma = \tilde{\Gamma}$, see supplementary material. In principle, fluctuations of the Rabi frequencies due to the thermal motion of the atoms would lead to dephasing, which we neglect here. This approximation is justified a posterior by the agreement of our model with the experimental data. Another dephasing mechanism arises from the change of the probe power along the atomic ensemble, which can be accurately modeled by consecutively solving the Lindblad master equation and computing the transmission coefficient of each three-level atom [21]. We numerically checked that our approach captures the dynamics well in the parameter regime studied here. Therefore, we simplify the description by assuming that the entire ensemble evolves according to the single-atom dynamics such that the transmission of the probe beam is given by

$$T_{\text{probe}}(t) = \exp \left[-\tilde{OD} \frac{\tilde{\Gamma}}{\tilde{\Omega}} v(t) \right]. \quad (5)$$

Here, \tilde{OD} is the optical depth for the probe field on the light-shifted two-photon resonance, and $v(t) = 2\Im(\rho_{ba})$, where ρ_{ba} is the off-diagonal element of the density matrix and $\Im(\dots)$ denotes the imaginary part. We find that $v(t)$ is given by

$$v(t) = \frac{\tilde{\Gamma} \tilde{\Omega}}{\tilde{\Gamma}^2 + \tilde{\Omega}^2} \left[1 - e^{-\tilde{\Gamma}t} \left(\cos \tilde{\Omega}t + \frac{2\tilde{\Gamma}^2 + \tilde{\Omega}^2}{\tilde{\Omega}\tilde{\Gamma}} \sin \tilde{\Omega}t \right) \right]. \quad (6)$$

3.3. Observation of oscillatory Raman gain and absorption

For the following measurements, we increase the coupling laser detuning to $\Delta_c \approx 2\pi \times 32.5(3)$ MHz and set $\Omega_c \approx 2\pi \times 28.2$ MHz. The probe Rabi frequency can be expressed in terms of the so-called beta factor. It is defined as $\beta = \Gamma_g/\Gamma$, i.e., the ratio between the atomic emission rate into the guided probe mode Γ_g and the total emission rate Γ of the atom [32]. With that, the probe Rabi frequency is

$$\Omega_p = \sqrt{\frac{5}{12} \frac{4\beta\Gamma P_p}{\hbar\omega_p}}, \quad (7)$$

where P_p is the input probe power. In order to increase the coupling strength of the atoms to the guided mode, β , we increase the red trapping power to 2.8 mW during the probing. This shifts the trapping minima closer toward the nanofiber surface and results in a coupling strength of $\beta \approx 0.015$. The probe power of ≈ 480 pW then corresponds to a Rabi frequency of $\Omega_p = 2\pi \times 6.5$ MHz. The corresponding intensity at the position of the atoms is 8.2 mW cm $^{-2}$.

We plot the measured time-dependent probe transmission for these parameters and ≈ 700 atoms in figure 3. During the first 200 μ s (not shown here), only the probe field is on, and we observe unity transmission. This is expected since the probe field does not couple to atoms in the initial state $|a\rangle$. We then turn on the coupling field at time $t = 0$ μ s for 1 ms. Since the initial state corresponds to full inversion of the effective two-level system, the transmission of the probe field first experiences Raman gain, and we observe a transmission coefficient of up to ≈ 2 . However, during the following coherent dynamics, the transmission oscillates between Raman gain and Raman absorption. After about two full oscillations, the system reaches a steady state. We fit the experimental data in figure 3 using equation (5) with $\tilde{\Omega}$, $\tilde{\Gamma}$, and \tilde{OD} as free fit parameters. The fit (orange solid line) agrees very well with the data for an effective Rabi frequency of $\tilde{\Omega} = 2\pi \times 2.63(3)$ MHz, in reasonable agreement with the estimated $\tilde{\Omega} = 2\pi \times 2.83$ MHz, based on independently calibrated parameters. The fit result $\tilde{\Gamma} = 2\pi \times 516(21)$ kHz is in good agreement with the expected value according to equation (3), $\tilde{\Gamma} = 2\pi \times 490$ kHz. By assuming that $\tilde{\Gamma} = \Gamma_{ee}$, we can infer an average excited state population of $\rho_{ee} = 0.100(1)$. For the optical density, we obtain $\tilde{OD} = 5.6(2)$. Using these fit results, we also calculate the dynamics of the population in state $|a\rangle$, given by ρ_{aa} (dashed red line in figure 3). The population dynamics exhibits an oscillation that is 90° out of phase with the probe transmission and that reaches a steady-state value of 0.481(4). The 90°-phase difference stems from the fact that T_{probe} is determined by the imaginary part of ρ_{ba} , which oscillates 90° out of phase with ρ_{aa} .

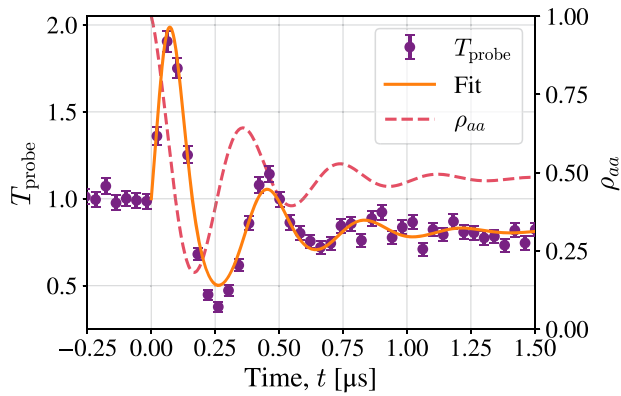


Figure 3. Dynamics of the probe transmission coefficient. At time $t = 0 \mu\text{s}$, we turn on the coupling laser. The ensemble then undergoes two-photon Rabi oscillations, evident by the oscillatory Raman gain of the probe (purple dots). The error bars are calculated assuming Poissonian counting statistics. We fit the data using equation (5) (solid orange line), yielding a two-photon Rabi frequency of $2\pi \times 2.63(3) \text{ MHz}$, in agreement with an estimate based on independent calibration measurements. Using the fit results, we also infer the average population in $|\alpha\rangle$ (dashed red line). The shown data is averaged over 2300 experimental runs.

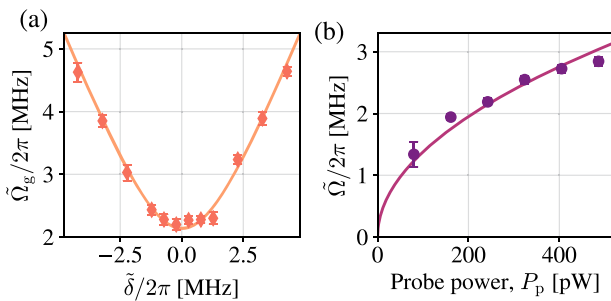


Figure 4. Scaling of the two-photon Rabi frequency $\tilde{\Omega}$. (a) For a two-photon detuning $|\tilde{\delta}| > 0$, we observe an increase of the oscillation frequency according to the generalized Rabi frequency $\tilde{\Omega}_g = (\tilde{\Omega}^2 + \tilde{\delta}^2)^{1/2}$ (orange diamonds). A fit (orange line) yields $\tilde{\Omega} = 2\pi \times 2.13(4) \text{ MHz}$. We average over 1000 experimental runs for each $\tilde{\delta}$. (b) Measured values of $\tilde{\Omega}$ as a function of probe power (purple dots) and fit using a square root function (purple line). We average over 2000 experimental runs for each probe power.

3.4. Scaling of the two-photon Rabi frequency

To gain more insight into the underlying physics of the two-photon Rabi oscillations observed in figure 3, we repeat the above measurement for different $\tilde{\delta}$ and plot the resulting fitted two-photon Rabi frequency in figure 4(a). These extracted Rabi frequencies can be very well described with the generalized two-photon Rabi frequency, $\tilde{\Omega}_g = (\tilde{\Omega}^2 + \tilde{\delta}^2)^{1/2}$. A fit (orange line) then yields an on-resonance two-photon Rabi frequency $\tilde{\Omega} = 2\pi \times 2.12(4) \text{ MHz}$ for this set of measurements. This is in reasonable agreement with the calculated $2\pi \times 2.0 \text{ MHz}$ for a probe power of $\approx 240 \text{ pW}$ used in this measurement.

In figure 4(b), we show the results of our experimental investigation of the dependence of $\tilde{\Omega}$ on the probe power. We observe that the two-photon Rabi frequency increases with

P_p , and we fit the data with a square root function, $A\sqrt{P_p}$, yielding $A = 2\pi \times 138(3) \text{ kHz}/\sqrt{\text{pW}}$. The fit curve (purple line) agrees very well with the data, as expected, given the square root dependence of the Rabi frequency on the power. Using our independent calibrations for Ω_c and Δ_c , we extract $\beta = 0.0171(8)$ from the value of A , in reasonable agreement with our expectation.

4. Conclusion and outlook

In summary, our system features an efficient and homogeneous coupling of the nanofiber-trapped atoms to the guided probe field. In conjunction with a large optical depth of the atomic ensemble on the two-photon resonance, this allowed us to study the oscillatory Raman gain and absorption associated with two-photon Rabi oscillations. In the present work, only the probe field was nanofiber-guided, giving us access to the gain and absorption dynamics of the latter. Launching both probe and coupling field through the nanofiber, as, for example, has been done in [15, 17], would yield the possibility to also measure the correlations between the probe and coupling fields, possibly even with single-photon resolution. Beyond shedding light on the fundamental processes underlying two-photon Rabi oscillations, our method could also be used to investigate the dynamical establishment of electromagnetically induced transparency.

Acknowledgments

We would like to thank M Fleischhauer for stimulating discussions and helpful comments. We acknowledge funding by the Alexander von Humboldt Foundation in the framework of the Alexander von Humboldt Professorship endowed by the Federal Ministry of Education and Research. LPY is grateful to the Department of Physics of Humboldt-Universität zu Berlin for his stay as a guest scientist.

Data availability statement

The data that support the findings of this study are available upon reasonable request from the authors.

ORCID iDs

Christian Liedl  <https://orcid.org/0000-0002-3518-4386>
 Sebastian Pucher  <https://orcid.org/0000-0001-5559-0114>
 Philipp Schneeweiss  <https://orcid.org/0000-0002-1485-7502>
 Leonid P Yatsenko  <https://orcid.org/0000-0002-2896-021X>
 Arno Rauschenbeutel  <https://orcid.org/0000-0003-2467-4029>

References

[1] Vitanov N V, Halfmann T, Shore B W and Bergmann K 2001 *Annu. Rev. Phys. Chem.* **52** 763–809

[2] Bergmann K, Theuer H and Shore B 1998 *Rev. Mod. Phys.* **70** 1003

[3] Arimondo E 1996 *Prog. Opt.* **35** 257–354

[4] Fleischhauer M, Imamoglu A and Marangos J P 2005 *Rev. Mod. Phys.* **77** 633–73

[5] Hau L V, Harris S E, Dutton Z and Behroozi C H 1999 *Nature* **397** 594–8

[6] Kozhekin A E, Mølmer K and Polzik E 2000 *Phys. Rev. A* **62** 033809

[7] Hatanaka H and Hashi T 1975 *J. Phys. Soc. Japan* **39** 1139–40

[8] Gentile T R, Hughey B J, Kleppner D and Ducas T W 1989 *Phys. Rev. A* **40** 5103

[9] Linskens A, Hollerman I, Dam N and Reuss J 1996 *Phys. Rev. A* **54** 4854

[10] Sheremet A S, Petrov M I, Iorsh I V, Poshakinskiy A V and Poddubny A N 2021 arXiv:2103.06824

[11] Nayak K P, Sadgrove M, Yalla R, Kien F and Hakuta K 2018 *J. Opt.* **20** 073001

[12] Solano P, Grover J A, Hoffman J E, Ravets S, Fatemi F K, Orozco L A and Rolston S L 2017 *Adv. At. Mol. Opt. Phys.* **66** 439–505

[13] Nieddu T, Gokhroo V and Chormaic S N 2016 *J. Opt.* **18** 053001

[14] Reitz D, Sayrin C, Mitsch R, Schneeweiss P and Rauschenbeutel A 2013 *Phys. Rev. Lett.* **110** 243603

[15] Sayrin C, Clausen C, Albrecht B, Schneeweiss P and Rauschenbeutel A 2015 *Optica* **2** 353–6

[16] Gouraud B, Maxein D, Nicolas A, Morin O and Laurat J 2015 *Phys. Rev. Lett.* **114** 180503

[17] Østfeldt C, Béguin J B S, Pedersen F T, Polzik E S, Müller J H and Appel J 2017 *Opt. Lett.* **42** 4315–8

[18] Meng Y, Dareau A, Schneeweiss P and Rauschenbeutel A 2018 *Phys. Rev. X* **8** 031054

[19] Corzo N V, Raskop J, Chandra A, Sheremet A S, Gouraud B and Laurat J 2019 *Nature* **566** 359–62

[20] Markussen S B, Appel J, Østfeldt C, Béguin J B S, Polzik E S and Müller J H 2020 *Appl. Phys. B* **126** 73

[21] Pucher S, Liedl C, Jin S, Rauschenbeutel A and Schneeweiss P 2022 *Nat. Photon.* **16** 380–3

[22] Vetsch E, Reitz D, Sagüé G, Schmidt R, Dawkins S and Rauschenbeutel A 2010 *Phys. Rev. Lett.* **104** 203603

[23] Schlosser N, Reymond G and Grangier P 2002 *Phys. Rev. Lett.* **89** 023005

[24] Bohren C F and Huffman D R 2008 *Absorption and Scattering of Light by Small Particles* (New York: Wiley)

[25] Mitsch R, Sayrin C, Albrecht B, Schneeweiss P and Rauschenbeutel A 2014 *Nat. Commun.* **5** 5713

[26] Dareau A, Meng Y, Schneeweiss P and Rauschenbeutel A 2018 *Phys. Rev. Lett.* **121** 253603

[27] Autler S H and Townes C H 1955 *Phys. Rev.* **100** 703–22

[28] Cohen-Tannoudji C N 1996 The Autler–Townes effect revisited *Amazing Light* (Berlin: Springer) pp 109–23

[29] Kumar R, Gokhroo V, Deasy K and Chormaic S N 2015 *Phys. Rev. A* **91** 053842

[30] Brion E, Pedersen L H and Mølmer K 2007 *J. Phys. A: Math. Theor.* **40** 1033

[31] Torrey H C 1949 *Phys. Rev.* **76** 1059–68

[32] Lodahl P, Mahmoodian S, Stobbe S, Rauschenbeutel A, Schneeweiss P, Volz J, Pichler H and Zoller P 2017 *Nature* **541** 473–80